Investigation into a Laser Welded Interconnection Method for Interdigitated Back Contact (IBC) Solar Cell Modules

by

Sujyot Sukumar Mony

A Thesis Presented in Partial Fulfillment
of the Requirements for the Degree
Master of Science

Approved July 2019 by the
Graduate Supervisory Committee:

Zachary Holman, Chair
Terry Alford
Zhengshan Yu

ARIZONA STATE UNIVERSITY

December 2019

ABSTRACT

Interconnection methods for IBC photovoltaic (PV) module integration have widely been explored yet a concrete and cost-effective solution has yet to be found. Traditional methods of tabbing and stringing which are still being used today impart increased stress on the cells, not to mention the high temperatures induced during the soldering process as well. In this work and effective and economical interconnection method is demonstrated, by laser welding an embossed aluminum (Al) electrode layer to screen-printed silver (Ag) on the solar cell. Contact resistivity below $1 m\Omega.cm^2$ is measured with the proposed design. Cross-sectional analysis of interfaces is conducted via Scanning Electron Microscopy (SEM) and Energy Dispersive X-ray Spectroscopy (EDXS) methods. Typical laser weld phenomenon observed involves Al ejection at the entrance of the weld, followed by Al and Ag fusing together mid-way through the weld spot, as revealed by cross-sectional depth analysis. The effects of voltage and lamp intensity are also tested on the welding process. With the range of voltages tested, 240V seems to show the least process variability and the most uniform contact between Al and Ag layers, upon using an Ethylene-Vinyl Acetate (EVA) encapsulant. Two lamp intensities were also explored with a Polyolefin (POE) encapsulant with Al and Ag layers seen welded together as well. Smaller effect sizes at lamp 2 intensity showed better contact. A process variability analysis was conducted to understand the effects of the two different lamps on welds being formed. Lamp 2 showed a bi-modal size distribution with a higher peak intensity, with more pulses coupling into the sample, as compared to lamp 1.

DEDICATION

I dedicate this thesis to my loving and supportive family, especially my parents Sukumar and Veena Mony, who have always been a constant source of guidance and motivation along my educational journey.

ACKNOWLEDGMENTS

I would like to thank my research advisor Dr.Zachary Holman for giving me the opportunity to conduct a master's thesis with him and his group. He has been very supportive and encouraging as a professor throughout the whole process. Through this thesis under him, I have truly learned what it means and what is expected of one to be a good researcher. His meticulous manner and methodical approach to working, are traits I hope that I can channel more thoroughly into my work in the future as well.

Secondly, I would like to thank Kathryn Fischer who has guided me throughout this whole process, without which this would not have been possible. Thirdly, I want to thank Kenneth Mossman and Karl Weiss, the research specialists at the Eyring Materials center, for their aid in sample preparation and microscopy related work for the thesis.

Lastly I would like to thank my friends and colleagues at ASU, Joe, Barry and Zach for their help and insight into my project.

TABLE OF CONTENTS

CHAPTER Page

Page

LIST OF TABLES

Table Page

LIST OF FIGURES

Figure Page

Figure Page

CHAPTER 1

INTRODUCTION

Background

Renewable energy is undoubtedly the future of global power generation. Traditional fossil fuel methods of generation are diminishing due to the long-standing climatic concerns, environmental damage and operating costs associated with their installation [1]. As of 2017, coal consumption in the U.S alone has decreased by 40% since 2005[2]. In contrast the largest drivers in variable renewable energy (VRE) over the last decade have been solar and wind energy sources. These sources are non-dispatachable and fluctuating in nature. Unlike other renewable sources like biofuel and biomass, the multiple steps of production are eliminated [3].

Although wind turbines possess a larger capacity to generate power, solar panel systems are easier to install, do not contribute to noise pollution and garner lower net costs when analyzing their energy output over a period of time[4,5]. This makes solar a more viable energy option for residential and commercial purposes.

In that regard, cost of the energy system is the principal driver in determining whether it will be implemented to serve the general American public or it's purpose on a utility scale. The goal stated by the U.S Department of Energy through their Sunshot initiative launched in 2011 was to make solar energy cost competitive with conventional means of electricity by 2020. Projected targets were set as 14% US electricity demand by solar in 2030 and 27% by 2050[6].

In aspiring to meet this goals, radical innovation in system-level science and technology along with increasing use of grid flexibility options, next generation power

electronics and other financial strategies was deemed to enable the U.S to get a significant portion of it's energy from solar, by 2020 and beyond [7]. Levelized cost of energy output(LCOE) is an indicator that plays a vital role when innovating with photovoltaic(PV) system engineered technologies[8]. LCOE($/W) is defined as the total cost to build an operate an energy system over it's lifetime divided by the sum electrical energy that the system will produce in it's lifetime[9,10].It is viewed as a measure to compare different methods of electricity generated by a power source consistently.

A study was conducted by Sunshot for PV systems in various U.S states, comparing LCOE across residential, commercial and utility scales(Fig.1). Projected cost targets were shown until 2020 and scenarios with federal investment tax credit were expected to decrease LCOE. A range of 1.1$/W to 1.6/W was the projected goal by 2020 observed from the study, based on the rate at which PV systems are have progressed. To meet such projected LCOE reductions, tradeoff between installed prices and other PV module characteristics such as module lifetime, degradation rate and efficiency must be made[8].

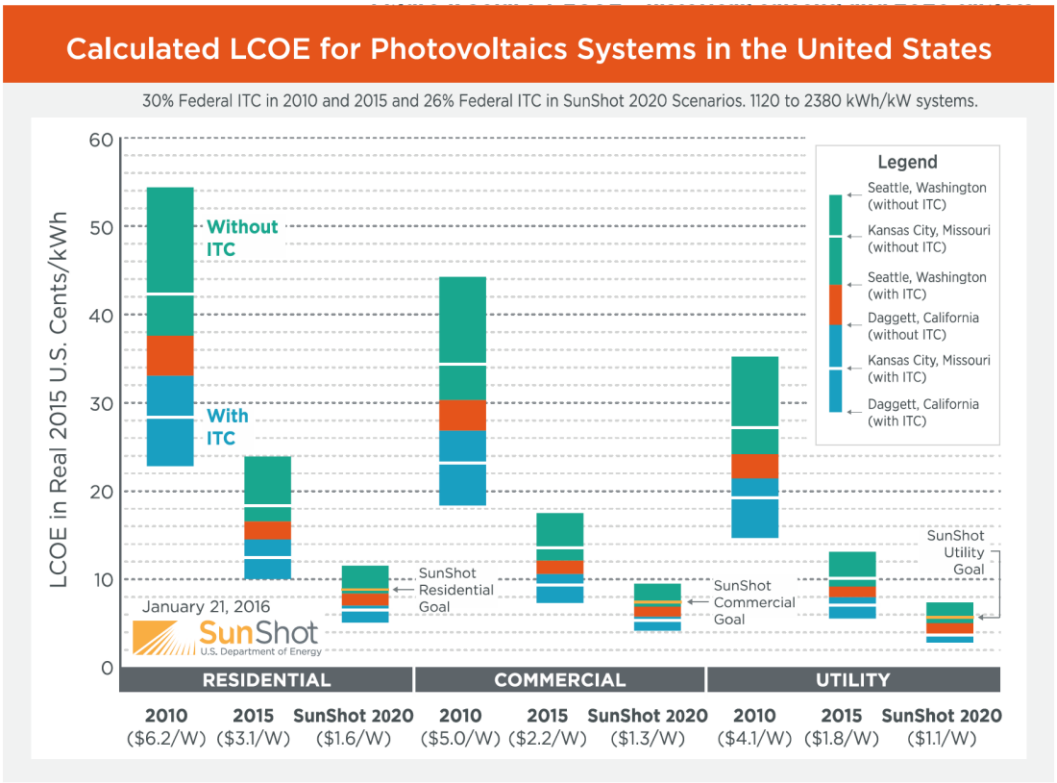

Fig.1: PV Levelized cost of energy(LCOE) in various states across the U.S ranging from residential, commercial and utility scale applications, 2010-2020. Cases assumed with and without ITC[7].

Therefore, the overarching goal of this work is to address the reduction in LCOE, by developing an efficient PV system technology. More specifically, we look at exploring the interconnection method in Interdigitated Back-Contact (IBC) solar cell modules as a means of improving overall efficiency in our system.

Motivation

Interdigitated back-contact (IBC) solar cells are among one of the many commercial solar cell types that exist in the market today. Their high cell efficiencies ranging from 22-26% make them prime candidates for mass production[11]. One of the

major problems however involved in the manufacturing of IBC modules lies in their interconnection method.

Commercially solar cells to date have been interconnected using traditional soldering methods. Stringing (tabbing) ribbon is used to electrically connect individual PV cells together (Fig.3). A bussing ribbon receives all this current to deliver it to a junction box for final electrical output. There are generally 20-80 PV cells connected to each other to constitute a complete module (Fig.2)[13].

a)

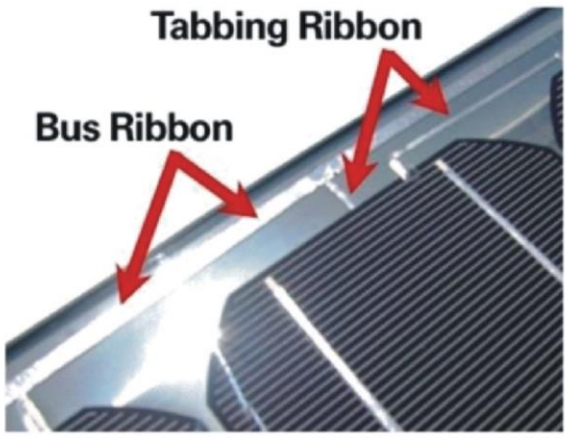

b)

Fig.2: a) Stringing and bussing ribbon serving as electrical connections between cells as well as to module. b) Full-sized module with interconnected solar cells[13]

However, the issue that arises in IBC modules is the fact that all stringing has to be conducted on the back of the cell, since the electrical contacts are located on the rear. Machines have to be adapted to solder tabbing ribbons in this way. Of more concern is the large mechanical stresses and CTE mismatch induced due to ribbon soldering, which causes the cell to bend or deflect downwards[14]. This phenomenon is referred to as “cell bowing”.

To overcome this phenomenon alternatives to the interconnection method are actively been researched such as electrically conductive adhesives (ECA), copper conductive backsheets[14]. Ultimately radical changes in the interconnection concept are required to make realizable steps of increasing energy conversion and power output of the cell over time.

Additionally a key area of concern in the manufacture of IBC modules is the high material costs associated with using copper whether it is for metallization or conductive backsheet purposes. Based on a study by Goris et al. at ECN solar energy, aluminum foil as a backsheet proved to be far more economical a proposition than using copper. The aluminum prices were cited as 1.24/kg compared to copper which was 5.25/kg(2014). Additionally aluminum when used as a backsheet performed comparably in reliability and cell to module loss testing as well[15].

As a result of these key insights, Dr.Holman's research group tested and compared the efficiency of three different interconnection methods namely: an embossed aluminum layer(before laser welding), copper conductive backsheets with ECA and finally the traditional tabbing metallization scheme mentioned earlier. It was found that the embossed aluminum design showed the highest power output with a fill factor (FF) of 76.8(Fig.3). The embossed aluminum design is patent pending and will be described in a later section.

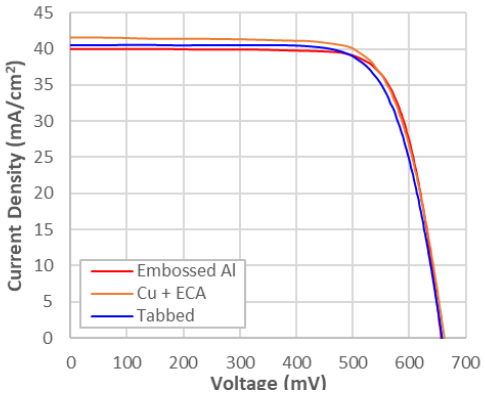

Module	Jsc	Voc	FF	Eff
Embossed Al	40.1	657	76.8	20.2
Cu + ECA	41.6	661	74.2	20.4
Tabbed	40.6	657	73.9	19.7

Fig.3: Power output comparison of various interconnection methods

Since embossed aluminum was the chosen material and interconnection layer of choice, the next step was to identify a method that could adequately form reliable mechanical and electrical contact from the IBC cell to module level. The idea of using laser welding as the interconnection scheme to investigate this issue stemmed from works that cite it as a loss and damage free module integration process [16]. Additionally laser welding has shown to produce low electrical contact resistivity's (ρ_c) below $0.01\Omega.cm^2$ when tested in Al-metalized Silicon solar cells; using Al foil with a silicone encapsulant to interconnect[17](Appendix A). Lastly, the reduced mechanical stress, high module tear-off stress and reduced process time have all been displayed with this technique on rear-contact cells [17].

Taking all these factors into account was the motivation to perform laser welding on IBC module structures, using an embossed aluminum layer as the cost-effective interconnect solution.

Research Goal

Therefore, the goal of this specific thesis however is to investigate whether a “laser welding” method (Refer to chapter 4) can help form a reliable mechanical and electrical bond between the silver busbars on the IBC cell to the aluminum electrode layer. A potential interconnect solution from cell to module is henceforth explored here. To do so we perform laser welding on the proposed module architecture by controlling process parameters and observing the effect on the results, all of which will be discussed in detail in later sections.

CHAPTER 2

IBC MODULE MANUFACTURING

IBC Solar Cell Design

There are many unique cell configurations used as mentioned earlier, to harness solar energy. Yet what makes the IBC configuration so unique is the fact that all contacts are placed on the rear side of the cell. This eliminates the idea of shading losses altogether and is a significant factor contributing to the high cell efficiencies [17]. Incoming photons (incident light) are absorbed in the front of the cell to create electron-hole pairs (carriers), which pass through the bulk and are consequently collected at the rear to generate current [18](Fig.4). The purpose of the passivation layers on either side of the substrate is to prevent the formation of dangling bonds, thereby reducing the number of recombination centers and contributing to a high-lifetime bulk region in the process.

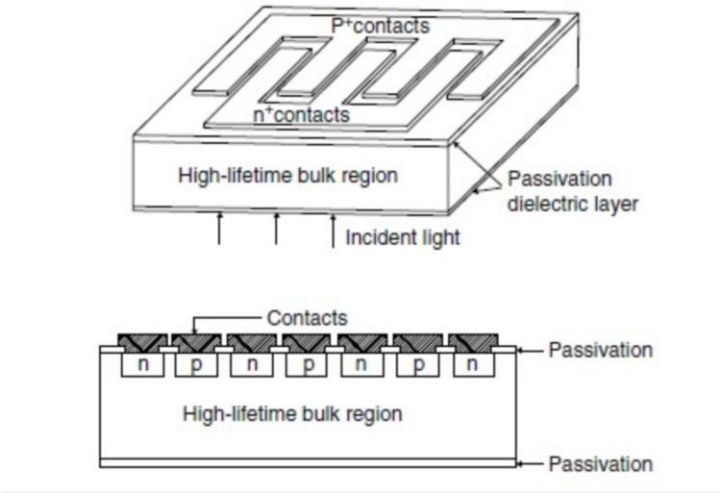

Fig 4: Standard IBC cell configuration[18]

Another advantage of rear contact positioning is that the amount of space that needs to be made or adjusted for light absorption would not be a big issue[18]. This allows for

easier interconnection since there is larger area occupied by the contacts and therefore lesser spacing between them. Additionally the contacts by occupying a larger area reduce overall series resistance in the cell[18], another major limiting factor to cell efficiency.

IBC Zebra Cell-Present State of the Art

The "Zebra" (IBC) cells as they are being called, developed in ISC Konstanz research institute have gained traction globally due to the fact that they are bifacial in nature. This enhances their power output even further. Currently the Zebra IBC cells are developed on $156\times156mm^2$ n-mono Si wafer(Appendix A) with a maximum conversion efficiency of 23%[19]. The modules have a double glass structure; they possess a low temperature coefficient of efficiency, immunity to humidity and excellent thermo-cycling properties[20]. Cutting edge production equipment used for processes such as tube furnace diffusion, laser opening of masking layers and screen-printing for metallization, make them strong candidates for manufacturing[19].

Proposed Module Design:

Currently a copper conductive backsheet with electrically conductive adhesive (ECA) has been actively been implemented and investigated in the interconnect research area, as mentioned in the earlier section. However the method proves to be more expensive than using Aluminum when cost-benefit analysis study was done for the manufacture of IBC modules. In this research developed at Dr. Holman's group at ASU, we have proposed on replacing the copper backsheet with a co-planar aluminum electrode layer in module design.

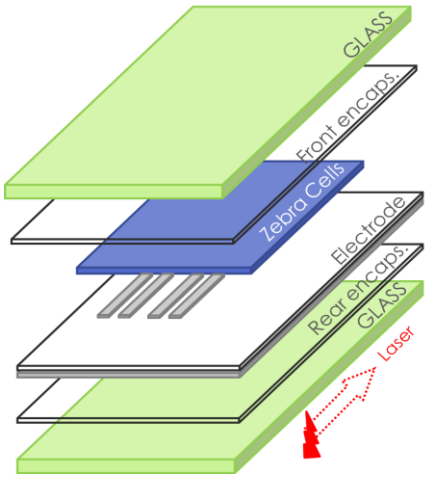

Fig.5: Laser welded module embodiment-front view

Therefore from Figure 5, we can see we have a glass-glass module design. Glass-glass modules were used after showing positive results in reliability testing such as impermeability to water vapor, less yellowing and discoloration, PID resistance and better aging behavior, to name a few [21]. The purpose of the encapsulant is similar, wherein it protects the cell form moisture intake, resists module to coloring and UV weathering as well as allows high power retention within structure [22].

As mentioned the uniqueness in this embodiment lies in the aluminum electrode. Essentially it is a 45µm layer of household foil that is laser inscribed with the embossed busbar pattern of the cell. The thickness of the foil was chosen based on standard IEC thermocycling tests (85^{o}C to -40^{o}C at 1^{o}/min), which showed that wrinkling of the foil occurred. Wrinkling is a positive indicator of the cell being degraded in reliability testing. The foil was scribed with laser to firstly create the soon to be isolated n-p contact regions. Secondly the foil was embossed with the busbar pattern on it using an embossing machine (Appendix A). The cell with busbars served as the die, which were then placed on top of

the patterned aluminum foil in the machine, to create the imprint. Each busbar was thus electrically isolated 2mm apart from each other in the process, to form the finished electrode layer(Appendix A).

The final architecture can be visualized as a zebra cell connected to an aluminum electrode layer, both of which are sandwiched in between an encapsulant and glass on either side(Fig.5).

CHAPTER 3

LASER WELDING-PHYSICAL PHENOMENA

Laser welding involves focusing a coherent, low-divergent optical energy source on a surface at high energy densities for a specified pulse duration. Power densities may range from 10^6-10^{14} W/cm^2 and pulse durations from continuous wave(CW) to femto-second(1fs=10^{-15}s)[23]. At the focal point of the weld, the localized material can undergo a series of physical processes such as heating, melting, evaporation, plasma formation and ablation[24]. In this section relevant laser absorption mechanisms and physical process phenomena at the weld area are described.

Laser Energy Absorption Process:

Upon a laser beam striking the material's surface part of the energy in the material is absorbed, the other part of the energy is reflected and the rest is transmitted[23]. Assuming metal to metal welding, ions constituting the lattice structure are too heavy to follow the oscillating electric field of the incoming laser radiation. Laser absorption in the metal hence occurs due to the presence of nearly free electrons. The nearly free electrons absorb laser radiation of all wavelengths at time scales of 10^{-16}s by an inverse "Bremsstrahlung" process[25]. Electrons share their energy through electron-electron collisions amongst other electrons. Since kinetic energies of electrons are high, temperature of the electron system increases. The electron energies are consequently shared with metal ions in lattice via electron-phonon interactions[26]. Upon actualization of the electron and lattice systems coming into thermal equilibrium, temperature of the material system on a whole rise.

Fresnel Absorption:

The complex refractive index determines the absorption characteristics in the material[27]. Mathematically the reflectivity 'R' at the surface is given by:

$$R=\{(n-1)^2 +k^2\}/(n+1)^2+k^2\} \quad 3.1$$

Laser radiation is permitted to be absorbed in metals due the free electron mechanism. These are opaque surfaces. This means that transmissivity is zero. Absorptivity is re-written as:

$$A=1-R. \quad 3.2$$

In simplified form:

$$A= 4n/\{(n+1)^2+k^2\} \quad 3.3$$

where α the absorption coefficient is given by:

$$\alpha = 4\pi k/ \lambda \quad 3.4$$

Laser radiation is absorbed along the depth(z) of the material and is expressed via the Beer-Ambert Law. I_0 and I(z) are the laser intensity at the surface and specified depth 'z' of the material, respectively.

$$I(z)= I_0\exp(-\alpha z) \quad 3.5$$

The 'skin depth' or 'absorption length' is a specified vertical distance within the material wherein the laser is absorbed and attenuated by a factor of exponential 'e'.

$$l_a = 1/\alpha = \lambda/4\pi k \quad 3.6$$

In most metals the imaginary part of the complex refractive index expression 'k' is usually larger than the real part 'n'. This means that reflectivity is greater, more than 90% generally, and the attenuation length is a few of 10nm [27]. General trends include decrease

in reflectivity and increases of absorptivity at shorter wavelengths for many metals. Additionally, the same holds true for reflectivity with increase of surface temperature[27].

Thermal Effect-Laser Interaction Zone:

Laser welding is a thermally driven process carried out with high intensity and short duration pulses. The temperature reaches a boiling point within a short period of time wherein heat conduction in the lateral and radial directions is negligible [28]. Therefore, assuming a 1-D heat conduction model, at the focal point of the material, the time of onset boiling for the material can be estimated using the equation:

$$\Delta T_0^* = 2(A.H/k)\sqrt{\kappa t/\pi} \quad 3.7$$

Where $\Delta T_0^* = \Delta T_0 + (L_f + L_v)/C_p$ is the rise in surface temperature; adjusted for heat of fusion and vaporization.

L_f= latent heat of fusion

L_v= latent heat of vaporization

C_p= specific heat

$H = P_1/\pi a^2$=absorbed laser power density

A=surface absorptivity

A=laser beam radius

k=thermal conductivity

κ=thermal diffusivity

t= time for onset of boiling during laser heating

Laser fluence is shown as Q=H.t ; therefore equation 3.7 is re-arranged as:

$$\Delta T_0^* = 2(A.Q/k)\sqrt{\kappa/t\pi} \quad 3.8$$

Equation 3.7 depicts the rise in temperature along depth of the material with respect to that of the surface. Equation 3.8 above depicts the proportionality of fluence 'Q' for ablation to $\sqrt{t}$, the time for onset of boiling during the heating process[28].

The depth $z= 2\sqrt{(\kappa t)}$ defined as the thermal diffusion length; is regarded as the distance a packet of heat energy is transported into the material upon time initiation of boiling. With 1-D heat flow assumption taken above we assume that the thermal diffusion length is smaller than the radius of the incident laser beam. To conclude, the overall effect of a laser pulse is determined by thermal diffusion length in the material, which is correspondingly dependent on the pulse duration[28,29].

Physical Processes-Laser Welded Zone:

In the case of lower intensities(10^6-10^9 W/cm^2), longer range- ms pulses, heat conduction as discussed, seems to be the dominant mechanism as a function of depth in the material. Ideally this mechanism applies to laser welding conducted at any timescales greater than 10ps as well. The rise in temperature at the laser interaction zone, depends on laser power density, laser pulse duration and thermo-physical properties of the material. Depending on the rise in temperature various laser weld phenomena may occur such as normal evaporation, normal boiling, melt ejection or phase explosion[30].

Normal boiling contributes to significant material removal at ms-μs duration scales based at the laser interacted area. In effect, a nucleation of heterogenous vapor bubbles occurs at a set boiling temperature. This occurs at a skin depth $l_a=1/ \alpha$, and corresponds to surface pressure[30,31].

Normal evaporation is another key process that can possibly occur at the ms timescale and power densities used. Over here a solid or liquid phase will transform to a

gaseous phase, with particles or atoms being seen emitted from the extreme outer surface[32]. On the other hand with the melt ejection process, upon initial evaporation, phase change from solid to liquid phase occurs i.e a molten liquid is formed. Additionally, upon evaporation a recoil pressure is exerted on the molten surface and if said recoil pressure exceeds the surface tension pressure of the molten liquid then radial ejection of liquid is seen and a hole is created[30,33]. Laser intensities are usually highest at the center, therefore temperature and recoil pressures are also highest at the center of the melt pool, rather than at the periphery. In effect vaporization is seen more vigorously, upon more of the laser energy that is absorbed and the deeper the hole that is created. Molten material can be ejected in the form of droplets, thin ribbon or even as spray along the wall of the hole[28,30].

Lastly at the final stages, laser pulse melt ejection is ceased, and the melt may either return as spatter or form a re-cast layer within the effect size that was created. Material removal in this case, occurs through vaporization and melt expulsion. However the fraction of material removal is dependent on the laser power and thermo-physical properties of the material[33,34]. The thickness of the liquid layer can be estimated by the thermal diffusion depth, which as mentioned earlier, occurs at the time onset for boiling.

Generally, melt ejection is dominant at low power densities. At higher power densities(10^9-10^{12} W/cm^2) and very short pulse length timescales, the vapor gets ionized to form a plasma plume[36]. The thermal energy deposition rate can supersede the vaporization rate leading to sub-surface super heating and pressure build up. Temperatures are higher than the boiling point, closer to the thermodynamic critical temperature, leading to homogenous bubble nucleation[36,37]. At the end of the lase pulse, superheated molten

material is ejected out in an explosive manner into a mixture of vapor and droplets, termed as ‘ablation’ [36].

CHAPTER 4

LASER WELDING INTERCONNECTION-PV MODULES

Laser welding although not a novel technique in photovoltaic module integration has however not quite yet thoroughly been explored in interconnecting IBC cells.

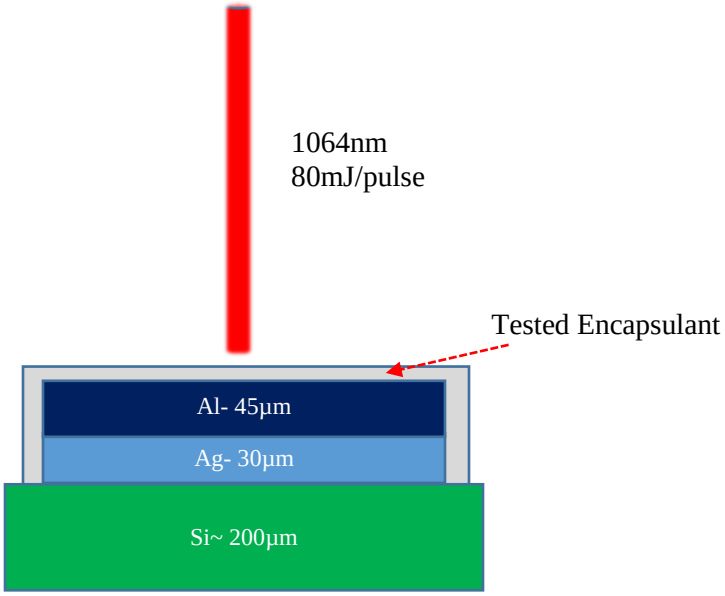

Fig.6: Laser-weld process schematic

Welding Approach:

The process we have incorporated is derived from the works of Schulte and Huxel's Aluminum-based Mechanical and Electrical laser interconnection (AMELI) process used for aluminum metallization on glass substrate [15,38,39,40](Appendix A). In our experiments however, a flash lamp pumped milli-second(ms) YAG laser was used to weld 45um aluminum foil to 35um screen-printed Ag, the busbars of the cell(Fig.6). The laser was run perpendicularly along the length of the module on the embossed busbars. The laser beam process was representative of a Gaussian or normal heat distribution model. Single pulses at a high fluence were used because of the reduced process time as well as the

potential damage free interaction observed between interfaces[38]. The laser welding of the modules was conducted by LaserStar a third-party vendor based in California.

Factors affecting Laser Welding Process:

There are four main independent process variables that affect properties of the weld spot formed, which are widely reported. These are the laser power, the incident laser beam diameter, pulse duration, material dependent absorptivity and the transverse speed of the laser across the substrate[22]. All other factors that are mentioned throughout literature are subsets of these main process variables or are closely inter-related to them. For instance in the works by Schulte, Huxel; pulse fluency, pulse duration, Gaussian beam radius and the central wavelength of the laser were some of the key factors accounted for, affecting the weld spot[38].

The spot size of a weld is governed by equation 4.1 below where Φ_0 represents the laser pulse fluence. Fluency is defined as the energy irradiated on the surface per unit area. E- the pulse energy and 'ω'- the Gaussian beam radius[38].

$$\emptyset_0 = \frac{2E}{\pi\omega_0^2} \qquad 4.1$$

In our study we wanted to vary parameters that have not been studied yet in literature. Hence, the effect of voltage and the effect of lamp intensity were the main parameters that were explored in this thesis.

CHAPTER 5

EXPERIMENTAL METHOD

In this chapter, the methods used to perform classical cross-sectional or micro-sectional failure analysis are described. The purpose of these methods is to mechanically expose the plane of interest in the PV package, so that interfacial interactions can be observed.

Sample Preparation

Cutting:

Samples were cut from the module using a powersaw with a silicon carbide(SiC) blade. The module was cut into rectangular pieces 8mm×2mm, so that they could be ready for epoxy encapsulation. Welds were made on top of the embossed busbar pattern as previously stated. Welds were chosen based on their weld size and parameters that may have affected the weld spot in the process. Proper sawing minimizes the area that needs to be grinded on, a later stage in this process.

Epoxy Encapsulation

Since we were interested in conducting an interfacial analysis of the PV module samples had to be potted in an epoxy puck. In general epoxy encapsulation serves the purpose of supporting the sample rigidly in place for clean exposure of the targeted area in grinding steps. The PV module under investigation contains different metallic layers. By potting the sample in a puck, care has to be taken to reduce charging effect from the epoxy puck.

To conduct the process 15 grams of epoxy resin were mixed with 1.8 gram of hardener, in a 100:12 resin hardener ratio. The solution was mixed well using a stirrer and

then placed in a vacuum oven(Appendix B) to remove air bubbles or trapped gas that would be involved in embedding. The resulting solution was then poured into a cylindrical moulded cup where sample was positioned at the bottom. The cup was then set in a chemical fume hood to allow the epoxy mix holding the sample to cure overnight. General curing time used for the experiments was 24 hours.

Grinding

After samples had cured, the epoxy puck was removed from the cylindrical moulded cup and ready for grinding. Grinding was performed on a Multiprep Allied tool(Fig.7). In effect the epoxy puck was attached to the holder either via silly putty or in certain instances melted wax. The side to be grinded on faced downwards towards the sandpaper.

Fig.7: General Multi-prep allied grinding and polishing tool

In our sample preparation, the sandpaper used was Silicion Carbide(SiC) ranging from a coarse grit size of 120um to a fine grit size of 1200um. It was placed on a platen with spin speeds used, varying from 65rpm-150rpm. Material was removed sequentially, with more material being removed at the initial stages with the coarse grit, with the intial aim being to flatten the sample. A 320um grit size was used to reach the target area i.e the laser welded area, followed by 600um grit to expose it. Larger scratches were removed in these instances. 800um and 1200um fine grit paper were finally used to eliminate smaller scratches prevalent on the surface. Generally, it followed that coarse grits were used for a shorter periods of time while the finer grits for longer periods since less material was removed.

Polishing

After grinding, polishing was done to remove the tiniest of scratches as well make the specimen plane highly reflective. The same Multiprep allied machine was in used in the process, however instead of sandpaper, polishing paper with diamond suspension was used as a replacement.

The process was initiated using a gold polishing pad as the abrasive surface. The pad was moistened with water and spun at 150rpm. A 15um water based diamond suspension was used as the abrasive solution. Lubricant was added whenever appropriate to smoothen the pad surface. After approximately 3 minutes the 15μm suspension was switched with a 6um diamond suspension, followed by a 1μm suspension on a white polishing pad. Final chemical polishing was performed on the same white pad with a 0.04um colloidal silica diamond suspension at 150 rpm.

Optical Microscopy

During grinding and polishing stages, the sample was constantly checked under the optical/light microscope to observe if scratches were indeed being removed from the sample and if the specimen was level. Such observations would give us insight into whether the grit size being used was appropriate or whether the sample had to be grinded or polished for a longer time. A Zeiss optical microscope was used with magnifications ranging from 10X-500X. 100X, 200X was typically used in our analysis. After a scratch free, deformation free and highly reflective viewing surface was obtained depicting the interfaces as a result of the laser weld phenomenon, the sample was ready for image capture. Additionally the microscope with it's in-built 'Quartz PCl' software was used to measure weld diameters needed for statistical analysis, described in a later section.

Materials Characterization

Sputtering:

To prepare samples for analysis in the SEM chamber, the sample i.e target area was coated with a gold, palladium(Au/Pd) coating. This was done to prevent charging effects, since the sample was encapsulated in epoxy, an insulating material. A sputter time of 55 seconds for was used to create an approximate 8nm coating. Consequently, carbon tape was then attached on either side from the metal layers on the sample edge, to the metal stub. This served to ground sample, providing and electrical pathway for them to flow away from the sample surface, as electrons from the incoming beam, would instigate electron repulsion, another way to induce a charging phenomenon [27].

Scanning Electron Microscopy (SEM):

Scanning electron microscopy (SEM) is based off the principle wherein a beam of electrons strikes the sample surface producing various signals that give us information about the topography and composition.

The electron beam passes through a series of lenses and apertures that focus the beam. The beam then hits a pair of scanning coils that deflect it so that it can be rastered in an x-y fashion on a rectangular area of the sample surface [28]. Electrons impinge upon the sample at various depths, there is energy exchange i.e scattering interactions occurring upon a desired teardrop shaped volume, known as the interaction volume. Electrons are then emitted and sent to the detector to create the desired image. The number of detected electrons is dependent on variations of the sample surface. The final electron image produced is therefore a result of the beam position and the intensity of the detected electrons[28].

Electrons which reach a depth approximately 10nm, i.e closer into the surface to produce a specific signal are classified as secondary electrons(SE). They result in generally high-resolution imaging. Electrons which reach deeper of approximately 0.5um are classified as back-scattered electrons(BSE) are used to detect areas of different chemical compositions. These are atomic number dependent.

In our analysis a NOVA 200-Nanolab FEI instrument was used with achievable resolution less than 100nm. An Everhart Thornley detector(ETD) was used for detection of SE, BSE(Appendix C).

Energy Dispersive Spectroscopy (EDXS):

Energy Dispersive X-ray spectroscopy (EDXS) is used for elemental and chemical characterization of samples [29]. Essentially, it is a technique based on X-ray excitation of the sample, but other technological variants such as excitation from protons and electrons are possible. Atomically speaking, an X-ray upon hitting the sample displaces an electron from the inner shell, leaving an electron hole or vacancy. An electron from the outer, higher-energy shell consequently falls in, to fill in the space that was left behind. The energy difference that occurs as a result of this is released in the form of an X-ray. The intensity of the emitted X-ray is measured by a spectrometer and displayed on our computers. Each element has their own unique atomic structure and therefore their own unique peaks on the electromagnetic emission spectrum [29].

The EDS detector was in-built on the NOVA-200 machine used for SEM imaging. NSS software was used for elemental and compositional analysis(Appendix C).

CHAPTER 6

DESIGN OF EXPERIMENTS ANALYSIS

The purpose of Design of Experiments (DOE) methods in is to identify important factors affecting the experimental response and to optimize that response**.** The state of statistical work can be described by initial data collection, data modeling followed by deciding which factors to choose for analysis. In this study the factors of interest were the voltage and lamp intensity of the laser used. The response variable was the laser weld spot diameter.

Linear Regression: Effect of Voltage on Weld Diameter

To understand the effect of voltage on weld diameter, voltages from a range of 220V-255V were chosen. The resulting weld spots created on the module were measured using "Quartz PCL" software, under the Zeiss optical microscope. A simple linear regression analysis was done to obtain the relationship(Fig.8). There is a positive correlation seen between voltage and weld diameter. As laser voltage increases, the size of the effect increases. A p-value of less than 0.05 indicates that voltage is a significant factor affecting weld size. Standard deviation was plotted for the set of data points as well, depicting process variability.

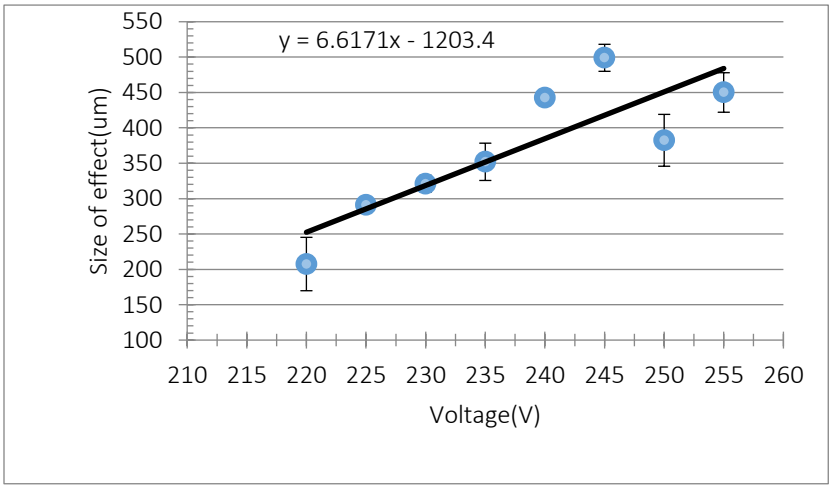

Fig.8: Bi-variate fit of weld spot diameter versus voltage

Table 1 Parameter Estimates for linear regression model for voltage vs weld diameter

Term	Estimate	Std error	t-ratio	Prob> |t|
Intercept	-1203.354	400.1902	-3.01	0.0238
Voltage	6.6170476	1.683054	3.93	0.0077

There was large variability seen at 220V, 235, 250V. Voltages of 225V, 230V and 240V, which showed the least variability, were the factors to be tested for characterization purposes.

ANOVA: Effect of Lamp Intensity on Weld Diameter

Laser welds were made along 8 busbars each, in two separate modules, for two different lamp intensities. Spot diameters were measured and the averages of the diameters for each set of busbars were taken. In total sixteen average diameters were calculated. A One way Analysis of Variance (ANOVA) analysis was conducted to study whether there was any significant difference between the two lamp intensities could be predicted, based off the spot diameters obtained (Table 2). A fixed effect model was used since the energy of the laser was held constant at 80mJ/pulse during the process.

Table 2 ANOVA for Lamp intensity factor a) Summary of fit b) ANOVA analysis c) Means for One-way Anova

R square	0.310075
Adj Rsqaure	0.260794
Root Mean Sqaure Error	44.06935
Mean of Response	504.4626
Observations(or Sum Wgts)	16

Source	DF	Sum of Squares	Mean Square	F ratio	Prob>F
Lamp Intensity	1	122219.844	12219.8	6.2921	0.0251
Error	14	27189.509	1942.1		
C.Total	15	39409.353			

Level	Number	Mean	Std.error	Lower 95%	Upper 95%
Lamp 1	8	476.827	15.581	443.41	510.24
Lamp 2	8	532.099	15.581	498.68	565.52

*Std.error uses a pooled estimate of error variance

A p-value of 0.0251, implies that there are significant differences in the both lamp intensities being used, making it an interesting factor to investigate on weld interactions. The mean weld diameter with a lamp 2 intensity seems to be higher compared to lamp 1, pointing to the fact that a higher intensity lamp, produces larger effect sizes.

CHAPTER 7

RESULTS AND DISCUSSION

In this section we explore the optimum way of conducting laser welding between the screen-printed silver of the cell and the 45um aluminum electrode layer through characterization and statistical methods. This was done so, by varying untested process parameters such as voltage and lamp intensity. Their effects are seen on the resulting welds to draw overall conclusions.

Macroscopic Phenomenon:

To begin, we wanted to observe the general macroscopic phenomenon of an interaction between aluminum and silver layers. EVA was used as an encapsulant between the aluminum and silver layers (Fig.9), in a glass-glass module structure. In this case there was no silver busbar pattern, however fingers were present. It was seen that Ag is macroscopically lumpy. Also, it was seen that the busbar did make contact with one of the fingers but was isolated from the other two fingers on either side, by the patterned encapsulant. Therefore it is was of interest to avoid a situation at all costs, wherein silver is not in contact with Al upon laser welding.

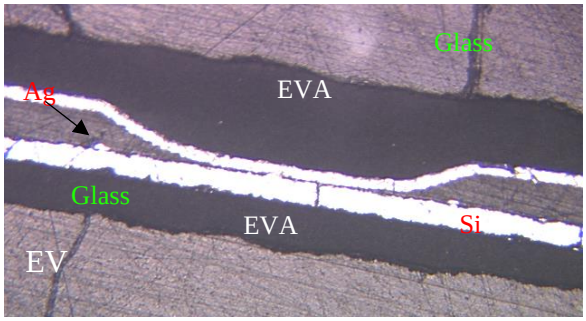

Fig.9: Cross sectional optical image with Ag finger and no busbar

We focus our attention to a laser-welded module now. A top down view of a laser-welded sample was taken. A photograph shows welding along the length of the busbar,

with isolation scribe separating each of the busbar regions(Fig.10a). A magnified view via an optical microscope image indicates spacing and positioning of welds more clearly(Fig.10b). A process alignment window was created to see the position along the busbar the weld was created. Stage speed and laser frequency was set up so that welds were positioned next to each other and not overlapping.

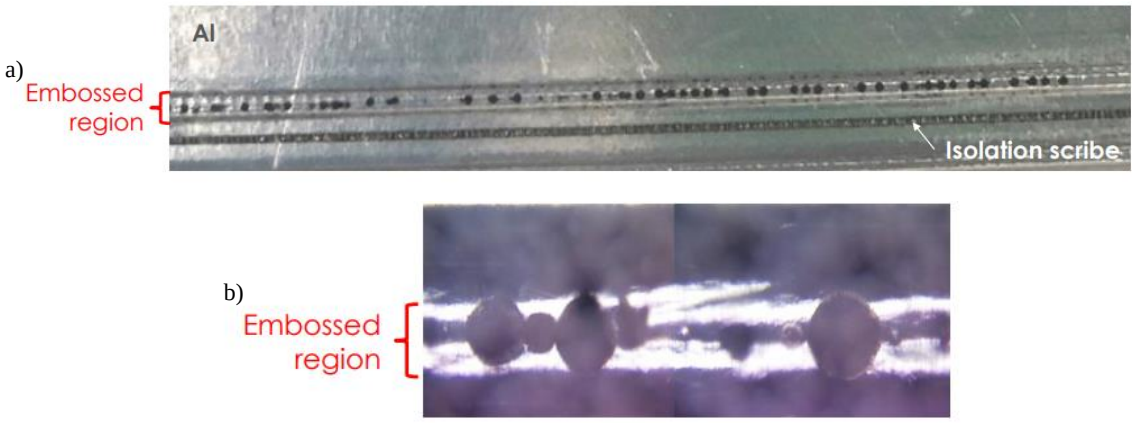

Fig.10: Laser weld spots on module a) top-down photograph b) optical microscope image

Microscopic Phenomenon:

Laser weld of Transmission Line Measurement (TLM) Resistance Structures

To see how the laser weld behaves with the encapsulant layers in place, transmission line measurement (TLM) structures were made and welded through the encapsulant layers. 30µm Ag lines are screen printed on top of the Si wafers, our solar cell, which was coated in silicon nitride. The cell is encapsulated under glass with EVA encapsulant- a cross-linking polymer that has the same refractive index and spectral absorption as glass. The welds are represented by the black dots in this case (Fig.11 a). Measurements were performed with milli-second YAG laser from here on in because of

unavailability of the quasi-continuous laser tool, which was used earlier. Energy from this point onwards was also held constant at 80mJ/pulse.

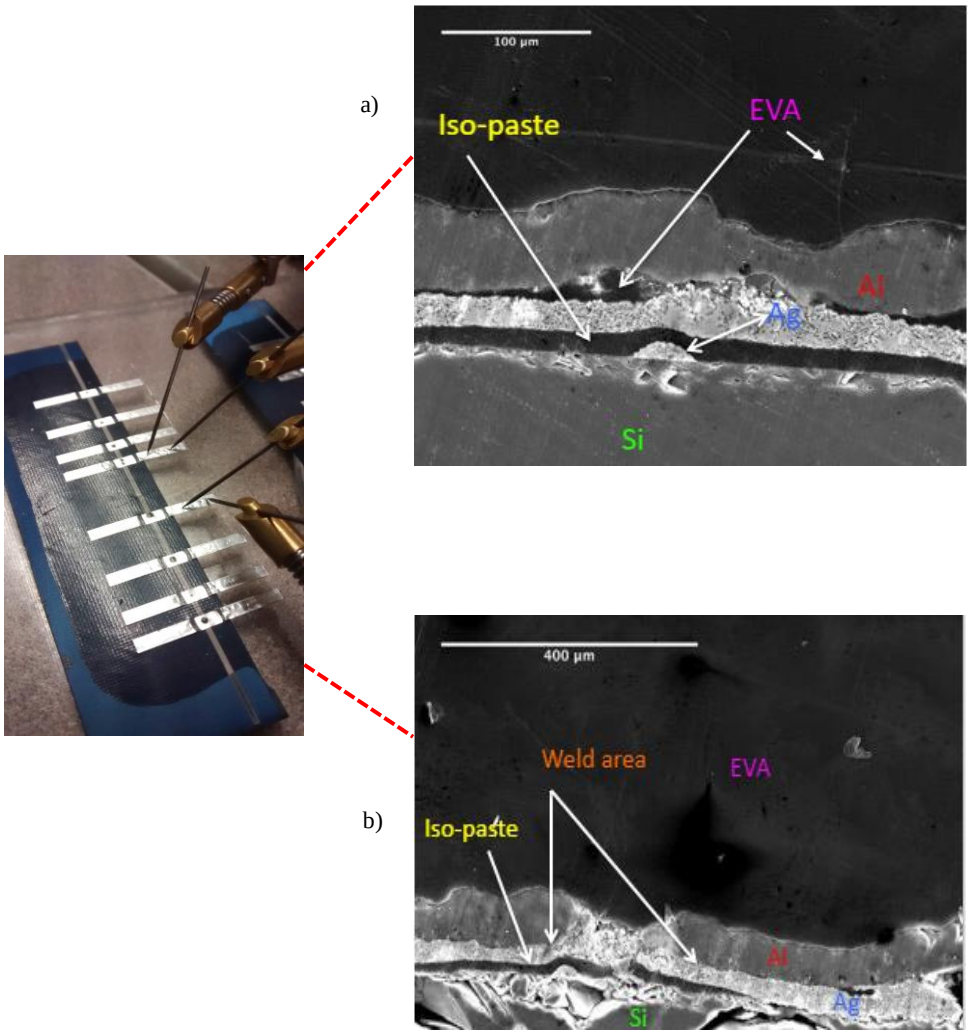

Fig.11: **a)** TLM resistance structure module b) SEM image of encapsulated TLM module i) pre-weld ii) welded area; 20kV, 0.62nA.

As can be seen via SEM imaging, the encapsulant served to isolate the foil contact pads (Fig.11b.i)(Appendix C). Upon hitting the welded area we do see Al and Ag layers fuse together as one would expect(Fig.11b.ii). In fact the contact is particularly consistent throughout. The EVA does a good job isolating the silver busbar from the finger as well. Additionally we note that since a weld is observable that the laser does indeed pass through

the EVA and glass structure corroborating the absorption spectrum data. Lastly, of worthy mention, is that no burning of EVA occurred, as no damage to the layer was observable, strengthening the idea of EVA being a stable encapsulant material for module packaging purposes. Damage to the Si layer underneath is observable and one of the aims of laser welding is to avoid such an occurrence, but at the same time still form a strong mechanical and electrical contact between the layers. However, in this case the damage visible in Si may more so be due to cracks in the cell or the increased pressure applied during the grinding process.

To see whether this was purely an experimental error, another sample was analyzed and this time a much cleaner electron image was obtained, with no damage to the Si. As mentioned in the experimental method, modules were cut up, cross-sectionally polished and imaged via SEM. These images similarly show a section of a Zebra cell where the Ag busbar is isolated from the finger running into the screen. The foil electrode is sitting on top of the Ag busbar and has been polished up to just in front of the weld. We wanted to see the effect upon hitting a weld spot.

a) b)

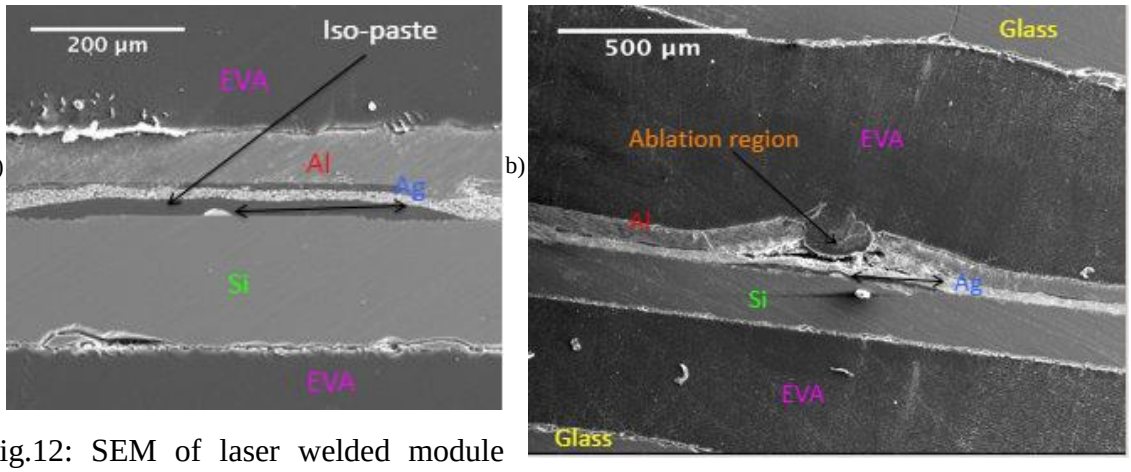

Fig.12: SEM of laser welded module structures a) Pre-Weld b) Welded area showing aluminum ejection;20kV, 0.62nA.

From works of Schulte and Huxel [25], it was observed that the energy required to weld thicker aluminum layers to silver was proportionally greater, a range from 7µm-20µm of those being tested on Al-metalized cells. This was attributed to the thermal expansion causing Al to be ejected from the melt before the entire thickness had heated through to the underlying substrate [25]. Therefore we wanted to see if this phenomenon of aluminum ejection held true in our structures.

Upon approaching the weld spot (Fig.12a) we see that the aluminum layer barely contacts the silver busbar. The layers are clearly distinguished, with the silver busbar curving upwards. However, as noted in literature, upon hitting the weld spot, we do see clear ejection of the aluminum layer (Fig.12b), a result of the localized heating of the laser beam. This is evident from SEM images above (Fig.12b), wherein large pieces of Al are removed. Additionally the first sign of contact between Ag and Al layers are seen, signifying that the welding is indeed possible using the proposed module design in this work.

To precisely understand layers and materials present at the weld area, a line scan was conducted (Fig.13).

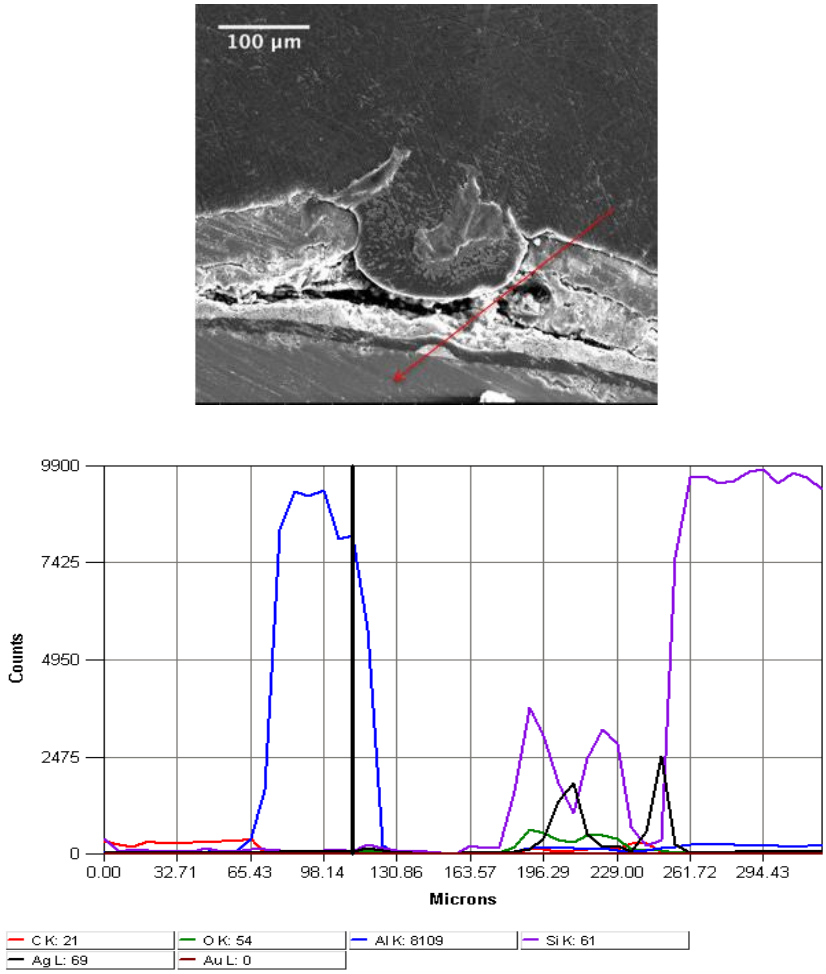

Fig 13: EDXS line scan along edges of weld effect

The EDXS line analysis identifies the different elements as function of depth in our sample. We initially start off at the EVA layer, shown by the low intensity carbon K-α energy. At around 65um we hit the Aluminum layer and consequently the two peaks at 200um, 260 um are representative of the silver busbar and silver finger. At 260um we hit the silicon cell. Between 200um-260um, we also obtain some X-rays from silicon; possibly indicating silicon precipitates diffusing into the welded region. EVA encapsulant also now fills in the void that was made via the aluminum ejection mechanism.

Impact of Weld Size:

Optical microscopy images were also taken at two different weld sizes, one considered a weld with a larger diameter and another one with a smaller diameter. With the smaller weld we find that silver busbar indeed stays intact(Fig.14a). However for the larger weld the laser completely ablates through both the aluminum and silver busbar, exposing the silver finger(Fig.14b).

a) 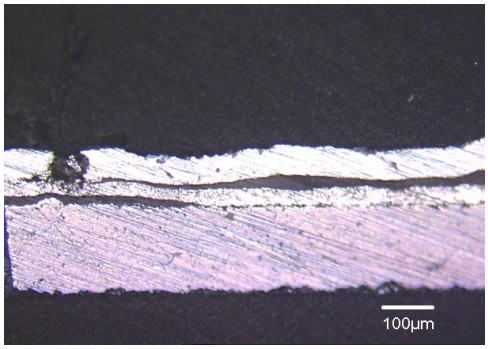

b) 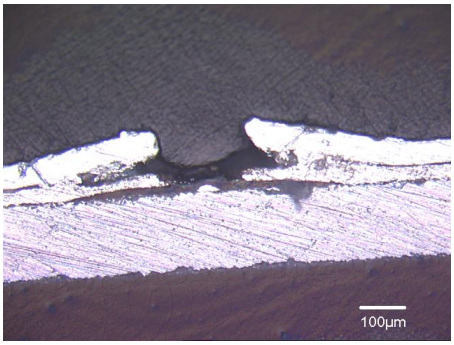

Fig.14: Module structure a) Small weld spot b) Large weld spot

From the optical images we conclude that that different interaction volumes can be achieved with the same laser. Therefore, our next area of investigation was to understand the influences of the laser's voltage on weld diameter.

Effect of Voltage on Laser Weld:

Based on a statistical analysis we conducted in the earlier chapter, it was decided to proceed with characterizing weld phenomenon at 230V and 240V, voltages that showed less process variability. 250V was also picked because weld phenomenon was of interest at one of the highest voltages in range. At 230V(Fig.15a) we came across a weld, however no contact between Al and Ag was seen. Similarly at 250V no contact was seen between the layers(Fig.15b). In fact the gap between the Ag and Al were quite discernable even at lower magnifications between 150X and 200X.

a)

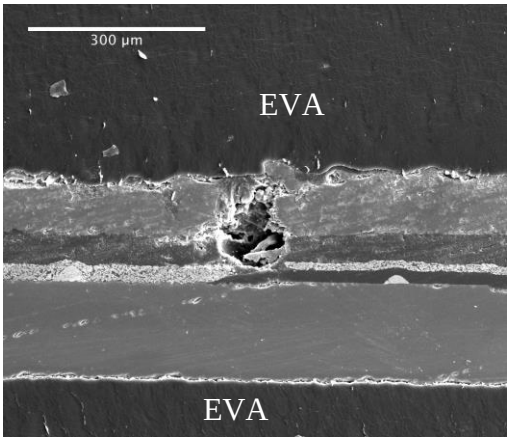

b)

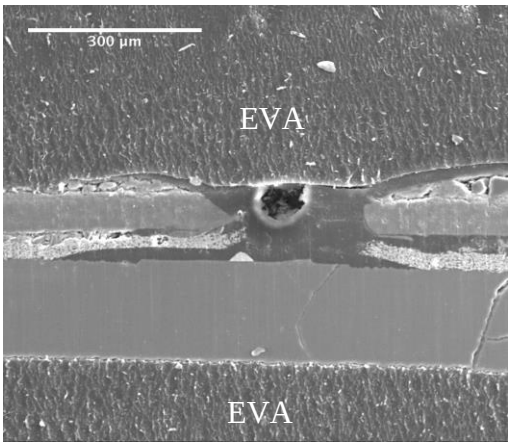

Fig.15: Weld spot at a) 230V b) 250V; 30kV, 0.63nA

However, at 240 V we observed quite the opposite phenomenon. Two different interaction volumes were imaged. For the case of spot 1(Fig.16a), a much larger weld area, great contact was seen at between the Ag busbar and Al at the weld . Along the sample itself the contact was more consistent. Also it was seen that the EVA encapsulant seemed to be merging into the cell at one of the weld spots and filling the void. The isolation paste also seemed to be preventing silver busbar and finger from contacting each other.

a-i)

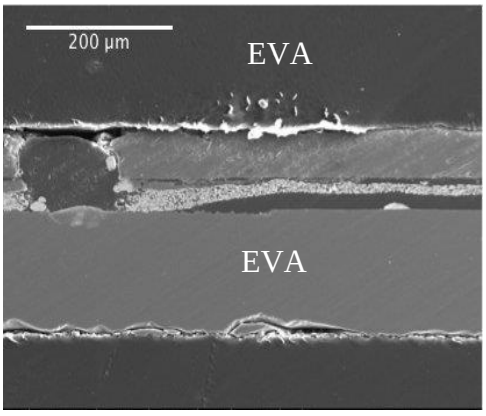

b-i)

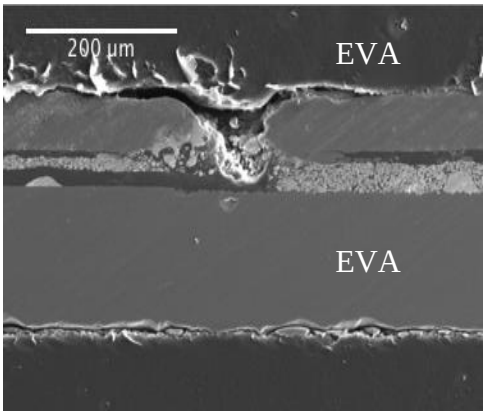

a-ii) 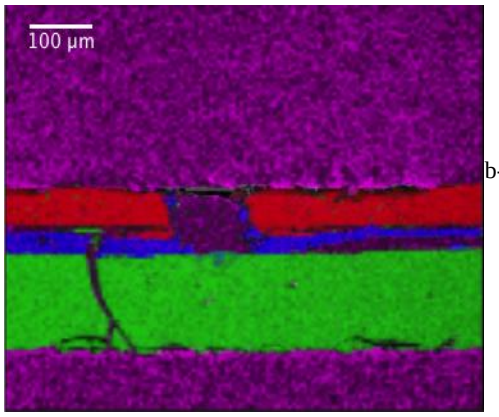

b-ii) 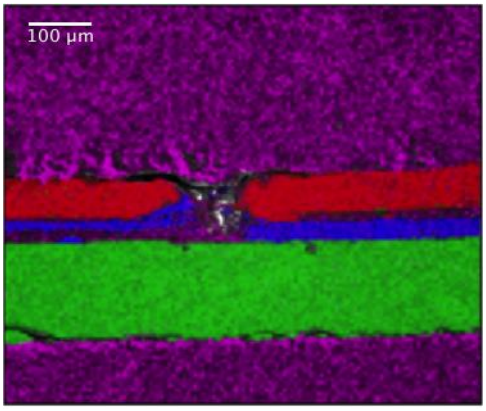

Fig. 16**:** a) Weld spot 1 at 240V i) SEM ii) EDXS b) Weld spot 2 i) SEM ii) EDXS; magenta=EVA, red=aluminum, blue=silver, green=silicon;20kV, 0.62nA.

For the case of spot 2(Fig.16b), a much smaller weld area was imaged. It was seen that aluminum and silver fused well together at the edges of the weld and silver was drawn up into the ablated region, a positive sign for interconnection. The isolation paste additionally served to protect the silver finger and silicon layer underneath. Since we discovered the optimum voltage for the process our next step was to then compare different lamp intensities.

Effect of Lamp Intensity on Laser Weld:

Two different laser-pumping lamps were used in this analysis. Lamp 2 had a narrower beam radius and therefore a higher intensity at the center. Lamp 1 conversely used a wider Gaussian beam radius to yield a lower intensity. As mentioned earlier, the laser welding process followed a Gaussian distribution model, and the laser intensity was representative of this model. The energy of the beam was kept constant through this process at 80mJ/pulse. Additionally POE encapsulant replaced EVA used in previous analysis.

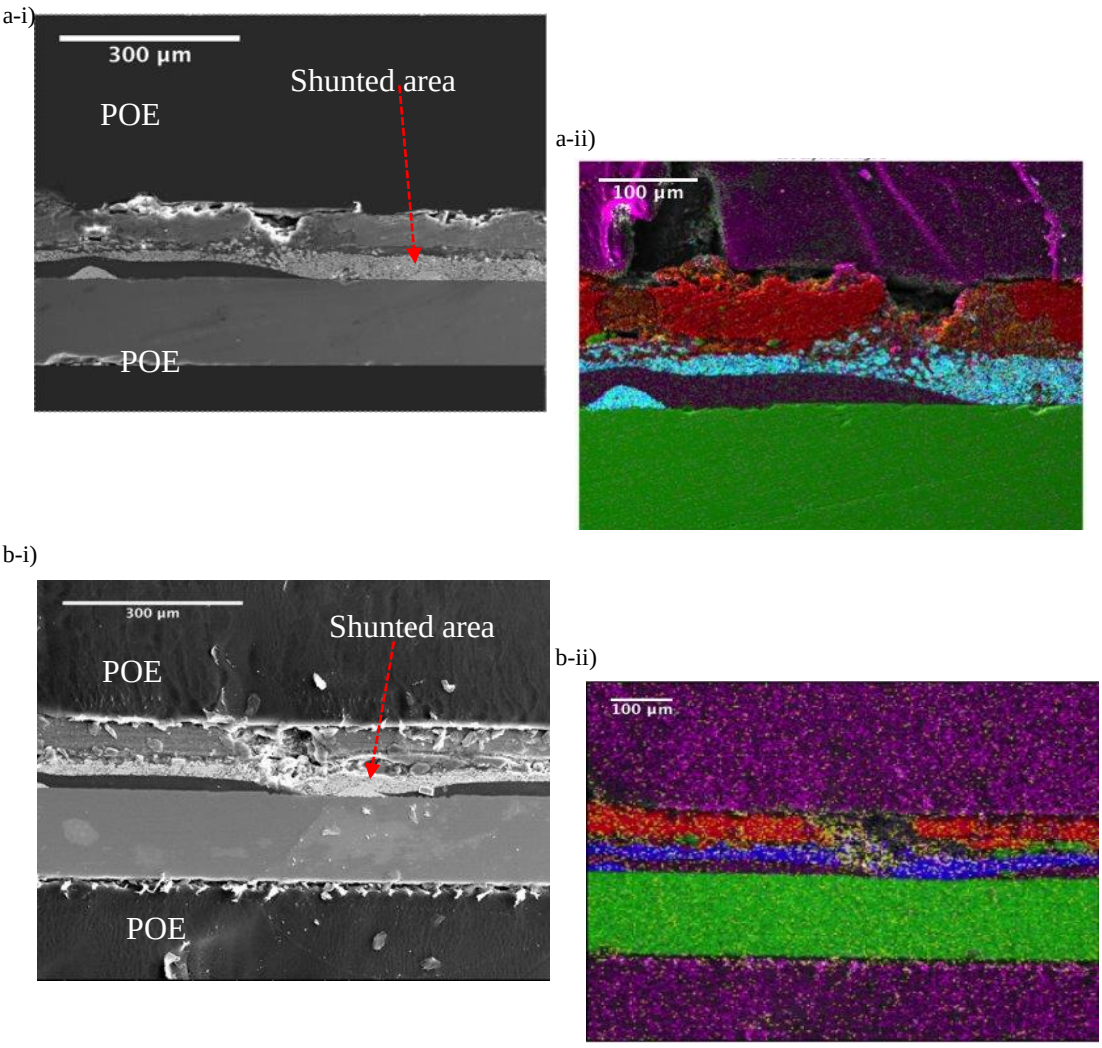

Fig.17 : Lamp 1 effect a) Weld 1 i)SEM ii)EDXS , 30kV, 9.5nA b) Weld 2 i)SEM ii)EDXS , 30kV, 2.4nA ; magenta=EVA, red=aluminum, blue=silver, green=silicon, yellow=oxygen.

Both a small weld (Fig.17 a) and medium sized weld (Fig.17 b) were imaged under Lamp 1. In both cases we observe previously described phenomenon. Both lamps seem to show clear contact between silver and aluminum layers at the weld area (Fig. 19). However upon further examination, contact between the silver busbar and finger is seen, leading to shunting of the cell. This is a kind of process condition one would want avoid at all costs during manufacturing. Shunt resistance leads to significant power losses in the cell, by

providing an alternate path for light generated current. Possibilities could be due to manufacturing defects which maybe corroborated by EL and PL imaging.

Consequently under Lamp 2 we imaged both a large weld (Fig.18 a) and small sized weld(Fig.18b). Contact was seen for both cases. For the larger weld, we notice breakage of the silver busbar, this could be attributed to the higher laser intensity used.

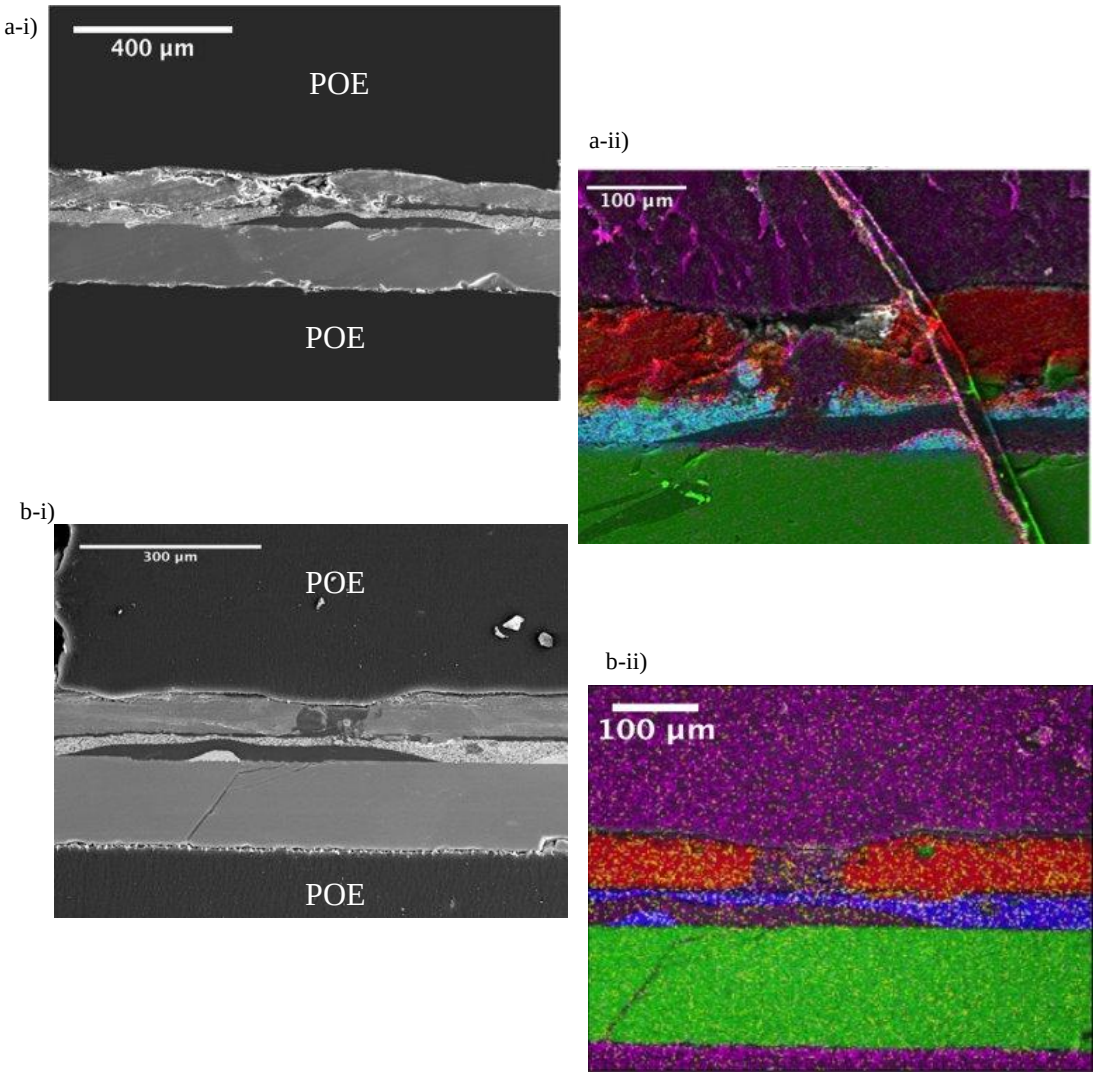

Fig.18 : Lamp 2 effect a) Weld 1 i)SEM ii)EDXS, 30kV,9.5nA b) Weld 2 i)SEM ii)EDXS, 30kV, 2.4nA ; magenta=EVA, red=aluminum, blue=silver, green=silicon, yellow=oxygen

With the smaller sized weld, no untoward phenomenon is observed, such as damage to the silver busbar or Si-cell, showing potential in the process, with welds at this size. Since it was established that welding is possible under both the lamp intensities using POE encapsulant, the next question for the analysis was to evaluate the optimality of each of the lamps used on the process overall. A process variability analysis was henceforth conducted to further the investigation.

Process Variability Analysis

Consequently, to gauge the process variability as a result of changing lamp intensities, two response variables were measured. The spot diameter was one, as mentioned in an earlier chapter. The second variable was the number of missing welds, essentially viewed as a spot where the laser had initially fired, but no weld had formed. These features were discernable under the optical microscope and counted. Similar to spot diameter, the number of missing welds was measured in the same modules previously used, along each of the eight busbars. The same measurement tools were used as well.

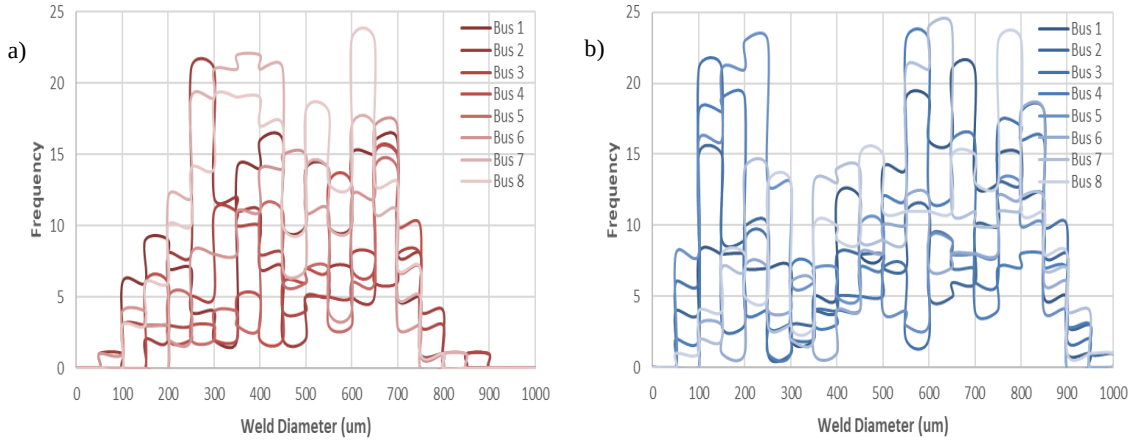

Fig.19: Weld diameter versus frequency on eight busbars processed with a) Lamp 1 b) Lamp 2 representative of Gaussian fit.

Firstly for the case of weld spot diameter, we observed that it varied greatly along each of the 8 busbars for both of the lamps that were used. Due to this occurrence, diameters were sectioned into bins and depicted via histogram-like plots (Fig.19). The weld diameters were plotted as a function of frequency; with the frequency representing the number of times a weld spot fell within a certain range of diameters. Additionally the frequency plotted against weld diameter was also representative of a Gaussian fit, similar to laser energy values plotted against diameter, in past literature works[25]. For the second lamp used, we observed the distribution was more bi-modal signifying a better frequency of an accurate spot size formed, in this case between 100-300µm and 500-700µm.

For case two, the number of missing welds, a higher percentage was observed along each of the eight busbars under Lamp 1(Fig.20). This implies that Lamp 2 had more pulses coupling into the sample. In effect this can be viewed as a positive occurrence because more points of contact can be initiated between the Al-Ag layers.

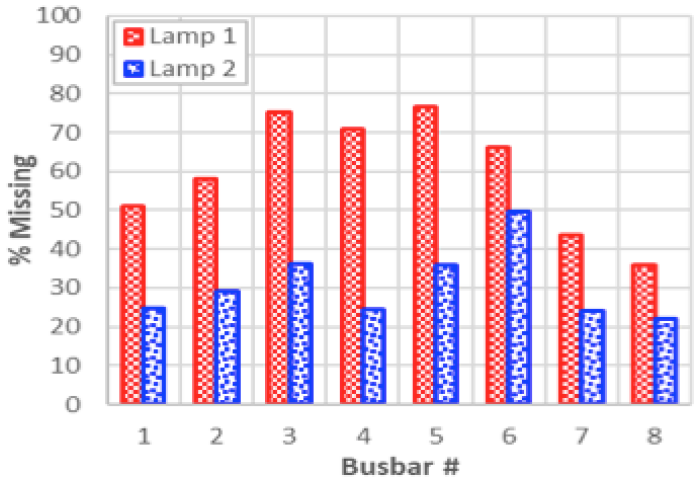

Fig.20: Percentage of missing welds versus busbar no. for lamp 1(red) and lamp 2(blue)

Cross-Sectional Depth Analysis:

After testing and validating the effects of voltage and lamp intensity on the weld phenomenon and process, our final step of this investigation was to perform a cross-sectional depth analysis (Fig.21). The purpose of doing so was do understand where exactly along the weld spot contact between layers was being initiated. Previously thus far, welds were being imaged upon contact been seen between Al and Ag layers, with no regards to position in the weld. To understand more precisely the microscopic phenomenon occurring as we grinded through the weld spot, was the aim of this analysis. We used the same process criterion for the module from our lamp intensity analysis, described in the last section, with POE as the encapsulant. In this case, the modules that were cut and encapsulated were from effect sizes produced by lamp 2, of higher laser intensity.

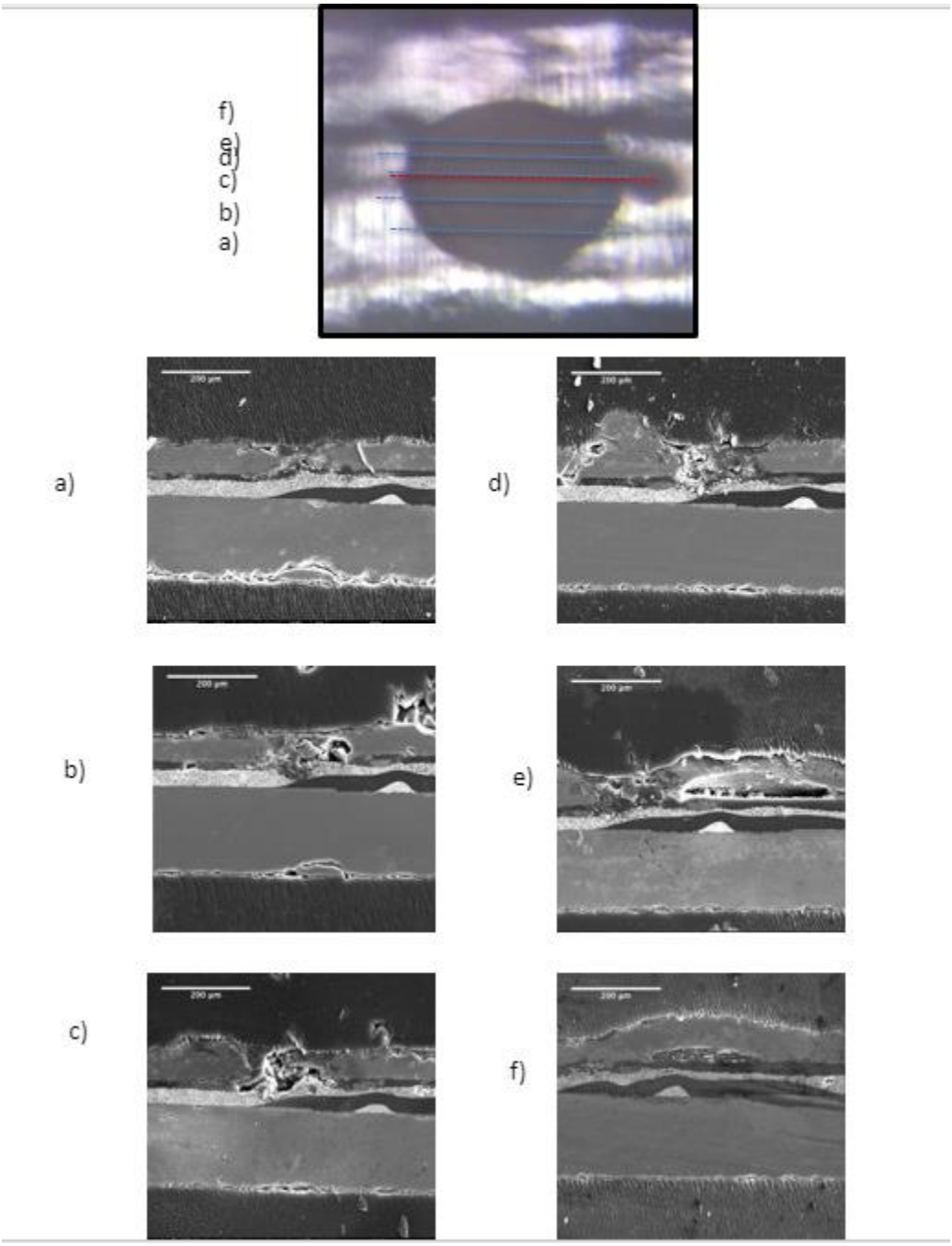

Fig.21: Cross-sectional depth analysis through a coupled weld at lamp 2 intensity a)-f) at 200X, E=30.0keV, I=0.63nA.

A series of snapshots were taken. As can be seen aluminum ejection is firstly seen upon entering the large weld spot(a). A little further past the entrance of the weld we now see that the silver busbar is damaged, possibly because we are moving to the region of the spot where laser intensity is more focused and localized(b). The amount of aluminum material ejected is greater at about halfway through the weld spot and it is at about this point we see more silver being drawn up into the ablated region and fusing with the Al at the edges(c). The widening of the weld area at this point could also be due to the fact we have hit the entrance of the smaller weld which has coupled into the larger weld spot. A little past midway approximately 30um out, contact is still seen(d). However 100um past the midway mark, the Al material that was initially removed starts to reappear(e). This is because we have moved further away from the spot at which laser intensity was the most concentrated. Fused Al and Ag at the edges are not seen anymore. Finally the Al seems to re-solidify and form a stable layer along the length of the busbar(f). POE is seen to isolate Al from the Ag busbar at this stage as well. The physical phenomena observed seem to be characteristic of vaporization and melt ejection processes described in Chapter 3.

A depth analysis was also done for a smaller weld size between two points. In this case just as seen earlier, the contact is seen midway through the weld spot. Past this point however, Al re-solidifies. A pore is also seen on the silver busbar, signifying a possible defect in the module manufacturing process.

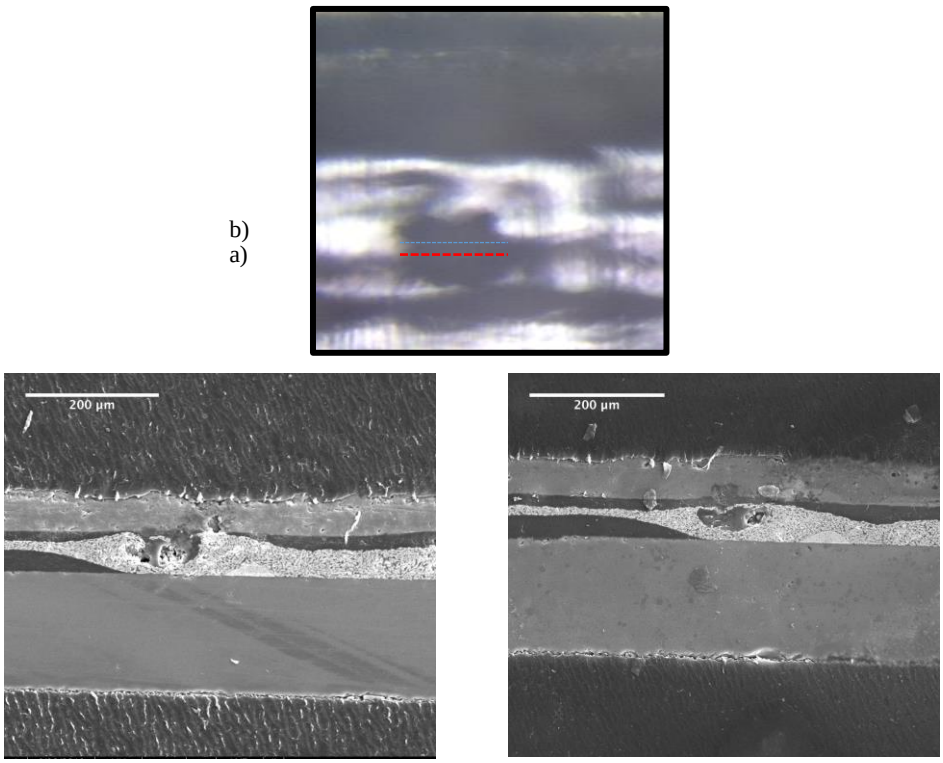

Fig.22: Depth analysis of a small weld spot at lamp 2 intensity a)-b) at 200X, E=30.0keV, I=0.63nA

CONCLUSION

Based on the investigation we have conducted, we determine that laser welding is definitely a possible interconnection option for Zebra Cell IBC module integration, using a 45um aluminum electrode design. Through electron imaging this was seen via aluminum ejection mid-way through the weld spot, as a result of localized heat of the laser, and fused silver-aluminum on the edges of the targeted area. Cross-sectional depth analysis revealed this to be the case. Voltages tested at 240V, using EVA encapsulant seemed to illustrate these phenomenon the best. This result seemed to validate linear regression analysis showing 240V as the least variable voltage through the range of voltages that were picked for the process, with effect sizes ranging from 420-460μm.

Upon imaging modules where two different lamp intensities were used as the variable factor, with a POE encapsulant, we found that welding in both cases was also possible. To determine which lamp intensity would be more optimal for use, we conducted a process variability analysis. Weld diameter and the number of missing weld were the two factors that were tested during the process. Lamp 2 of higher peak intensity and narrower beam radius showed a bi-modal distribution, when weld diameter was plotted as a function of frequency. Additionally the number of missing welds was reduced compared to a lamp 1, signifying more pulses coupling into the sample. Cross-sectional depth analysis was also done on a small weld and great contact was seen between Al and Ag layers.

To conclude overall feasibility of the laser welding process discussed here, power loss measurements and electroluminesce (EL) imaging for each of the module conditions would have to be performed and compared with results obtained from this thesis. Additionally thermo-cycling factors would have to be taken into account with module

testing. Nevertheless proof of concept of interconnection has been seen and other factors such as laser energy, pulse fluence and Gaussian beam radius could be tested under the proposed module design, to gather a broader spectrum of data on the process.

REFERENCES

1) "The Hidden costs of Fossil Fuels", Union of Concerned Scientists, August 30th.2016, www.ucsusa.org/clean-energy/coal-and-other-fossil-fuels/hidden-cost-of-fossils

2) Michael.Mobilia, "Petroleum, natural gas and coal still dominate U.S Energy consumption", U.S Energy Information Administration (eia), July 3rd.2018, www.eia.gov/todayinenergy/detail.php?id=36612

3) Ames.Hayley, "The Advantages & Disadvantages of Biomass Energy", March 13th.2018,https://sciencing.com/advantages-disadvantages-biomass-energy-8224681.html.

4) "Wind vs Solar: A head to head comparison", Arcadia Power, www.arcadiapower.com/energy-101/energy-sources/wind-vs-solar-a-comparison/

5) Sendy, Andrew. "Is solar or wind a better way to power your home?",Solar Reviews, April 30th.2018, www.solarreviews.com/blog/is-solar-or-wind-a-better-way-to-power-your-home

6) Woodhouse.Michael, Rebecca Jones-Albertus, David Feldman, Ran Fu, Kelsey Horowitz, Donald Chung, Dirk Jordan, and Sarah Kurtz. 2016. "On the Path to SunShot: The Role of Advancements in Solar Photovoltaic Efficiency, Reliability, and Costs". Golden, CO: National Renewable Energy Laboratory. NREL/TP-6A20-65872. www.nrel.gov/docs/fy16osti/65872.pdf

7) "On the Path to SunShot: Executive Summary", Solar Energy and Technologies Office of U.S Department of Energy(DOE). May 2016. energy.gov/sunshot. DOE/EE 1412. www.energy.gov/sites/prod/files/2016/05/f31/OTPSS%20-%20Executive%20Summary-508.pdf

8) "Comparing the costs of Renewables And Conventional Energy sources", Energy innovation Policy and Technology LLC, February 7th 2015. energyinnovation.org/2015/02/07/levelized-cost-of-energy/

9) "Are Existing Power plants less Expensive than New Gas, Wind or Solar?" America's Power(ACCCE), August 12th 2018. http://www.ourenergypolicy.org/wp-content/uploads/2018/08/LCOE-Levelized-Cost-of-Electricity-Report.pdf

10) "Levelized Cost of energy (LCOE)", DOE Office of Indian Energy. www.energy.gov/sites/prod/files/2015/08/f25/LCOE.pdf

11) Green.M.A, K.Emery, Y.Hishikawa, W.Warta, and E.Dunlop. 2015. "Solar cell efficiency tables". Progress in photovoltaics: research and applications, Vol.23, no.7, 805-812.

12) PFluke. Karl, “Soldering Photovoltaic Cells”, TECHNI-TOOL,Indium Coroporation, http://www.techni-tool.com/site/ARTICLE_LIBRARY/Indium%20-%20Soldering_Photovoltaic_Cells.pdf

13) Popovich V.A, Janssen.M, Bennett.J, Richardson I.M, Van Maris M.P. “Understanding properties of Silicon Solar cells and Aluminum Contact Layers and its Effect on Mechanical Stability” Materials Sciences and Applications, 2013. Vol.4, 118-127.

14) Maurice J.A, A.Goris, Ian.J Bennett, Wilma Eerentsetin, “Aluminum foil and cold-spray copper technology as cost reduction process step in back-contact module design”, Energy Procedia, 2014. vol 55, 342-347.

15) Schulte-Huxel.Henning, Blankemeyer.Sussanne, Merkles. Agnes, Bock.Robert, Brendel, Rolf. “Aluminum-based Mechanical and Electrical Laser Interconnection process for Module Integration of Silicon Solar Cells”. Institute for Solar Energy Research(ISFH), IEEE Journal of Photovoltaics, January 2012. Vol.2, no.1, 16-21

16) Schulte-Huxel.Henning, Blankemeyer.Sussanne, Merkles. Agnes, Bock.Robert, Kajari-Schroder.Sarah, Brendel.Rolf. “Al foil on encapsulant for the interconnection of Al-Metallized Silicon Solar cells” Institute for Solar Energy Research(ISFH), IEEE Journal of Photovoltaics, January 2013. Vol.3, no.1, 77-82.

17) Honsberg.C, Bowden.S, “Rear Contact Solar Cells”, www.pveducation.org

18) “What is IBC Solar cell technology?” In Style Solar. September 2018. www.instylesolar.com/blog/2018/09/27/ibc/

19) Halm.Andreas,Schneider.Andreas, Mihailetchi.Valentin, Libal.J et al.“Evaluation of cell to module losses for n-type IBC solar cells assembled with state of the art consumables and production equipment” International Solar Energy Research Center(ISC) Konstanz , IEEE PVSC, June 2013. Vol.39, 2368-2372.

20) “SunPower IBC Cell:Process Flow”, Youtube, uploaded by nanolearning, 5th May 2013, https://www.youtube.com/watch?v=5Jny4t4U4gI

21) Zachary Holman slide, “Literature Review: Reliability of Glass/Glass Modules with TPO encapsulant”, 2018. Arizona State University.

22) Webber.Tim, Lieb.Thomas,Mazumdar.J, “Welding Fundamentals and Processes-Laser Beam Welding”, ASM Handbook, 2011. Vol.6A, 556-569.

23) Steen.W.M, Mazumder.J, Laser Material Processing, 2010. 4th ed.

24) Spalding.I, Modern Laser Applications. Proc. Inst. Mech. Eng, 1987. Vol. 201,no.3, 165-174.

25) Yao.Y.L, Chen.H, Zhang.W, Time Scale Effects in Laser Material Removal: A Review, The International Journal of Advanced Manufacturing Technology, 2005. Vol.26, no. 5-6, 598-608

26) Satta.M, Ermer.D.R, Papantonakis.M.R, Flamin.C, Richard.F, Haglund.R.F, "Time Resolved Studies of Electron-Phonon Relaxation in Metals using a Free-Electron Laser. Appl. Surf .Sci, 2000. 154-155;172-178.

27) Ready.J.F, Industrial Applications of Lasers, Academic Press: New York, 1978. pp.354

28) Nath. A.K, "Laser Drilling of Metallic and Non-Metallic substrates", Comprehensive Materials Processing, 2014. Vol.9, 115-175.

29) Weber. R, Graf.T, Berger.P, Volkher.O, Wiedenmann.M, Freitag.C, Feuer.A, "Heat Accumulation during pulsed laser materials processing", Optics Express, University of Stuttgart, 2014. Vol.22, no.9.

30) Kannatey-Asibu, E.Jr, Principles of Laser Materials Processing, Wiley: New Jersey 2009.

31) Von Allmen.M, "Laser Drilling velocity in Metals", Journal of Applied Physics, 1976. Vol.47, 5460.

32) Anisimov.S.I, Khokholov.V.A, "Instabilities in Laser-Matter Interaction", CRC, Russian Academy of Sciences, CRC, Boca Raton, Fl, 1955.

33) Mazumder.J, Chan.C, "One-Dimensional Steady State model for damage by vaporization and liquid expulsion due to laser matter interaction", Journal of Applied Physics, 1987. vol.62, no.11, 4579-4586.

34) Low.D..K.Y, Li.L, "An Investigation into Melt Flow Dynamics during repetitive Pulsed Laser Drilling of Transparent media". Opt Laser Technol, 200. 33, 515-522

35) Dahotre.N.B, Harimkar.S.B, Laser Fabrication and Machining of Materials; Springer, 2008.

36) Leitz.K.H, Redlingschofer.B, Reg.Y, Otto.A, Schmidt.M, "Metal Ablation with short and Ultrashort Laser Pulses', Physics Procedia, 2011. Vol.12, 230-238.

37) Bulgakova.N.M, Bourakov.I.M, "Phase explosion under Ultrashort Laser Ablation: Modeling with Analysis of Metastable State of Melt.Appl.Surf.Sci, 2002. 197-198, 41-44.

38) Schulte-Huxel.Henning, Blankemeyer.Sussanne, Kajari-Schroder.Sarah, Brendel.Rolf, "Laser microwelding of thin al Al layers for interconnection of crystalline silicon Solar cells: analysis of process limits for ns and us process

lasers", Institute for Solar Energy Research(ISFH), Journal of Photonics for Energy, 2014. Vol.4, 041597(1-14).

39) Schulte-Huxel.Henning, Blankemeyer.Sussanne, Steckenreiter.Verena, Kajari-Schroder.Sarah, Brendel.Rolf, "Laser Welded Interconnection of screen-printed Si Solar cells", Institute for Solar Energy Research(ISFH), Energy Procedia, 2014. Vol.55, 356-360.

40) Schulte-Huxel.Henning, Blankemeyer.Sussanne, Kajari-Schroder.Sarah, Brendel.Rolf, "Analysis of Thermal Processes driving Laser welding of aluminum Deposited on Glass substrates for Module Interconnection of Silicon solar cells", Institute for Solar Energy Research(ISFH), IEEE Journal of Photovoltaics, November 2015, Vol.5, no.6, 1606-1612.

41) Chang.Long, "SEM Sample Charging", Pythography, 2018. http://www.pythography.com/sem/charging.html

APPENDIX A

EMBOSSING PROCESS-IBC MODULE

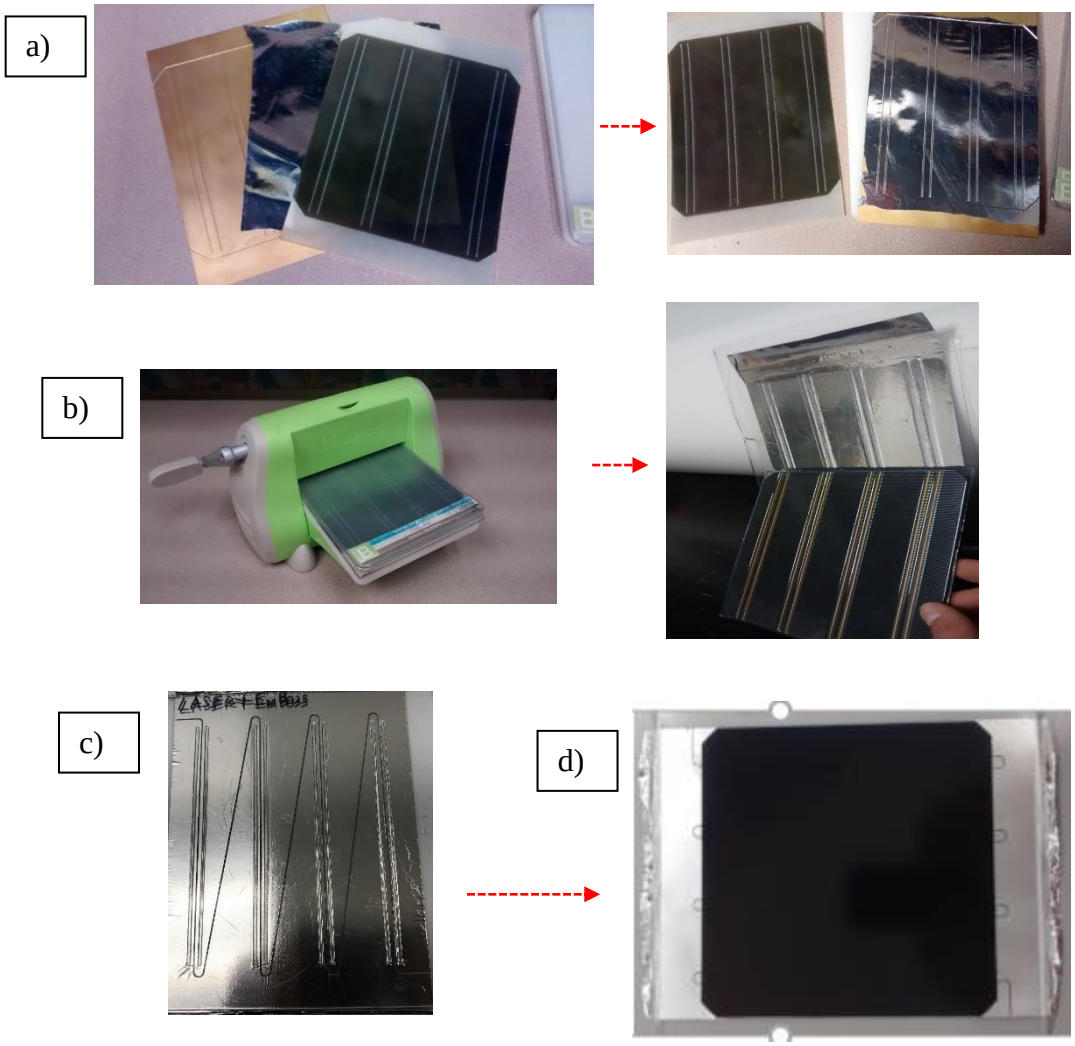

Embossing process: a) 3 layer arrangement- cell with encapsulant and stencil b) Embossing machine used for imprint c) Result of embossment followed by laser patterning to isolate contact regions-electrode layer d) 156mm×156mm back contact cell attached to electrode to constitute-finished IBC module.

APPENDIX B

SAMPLE PREPARATION SETUP

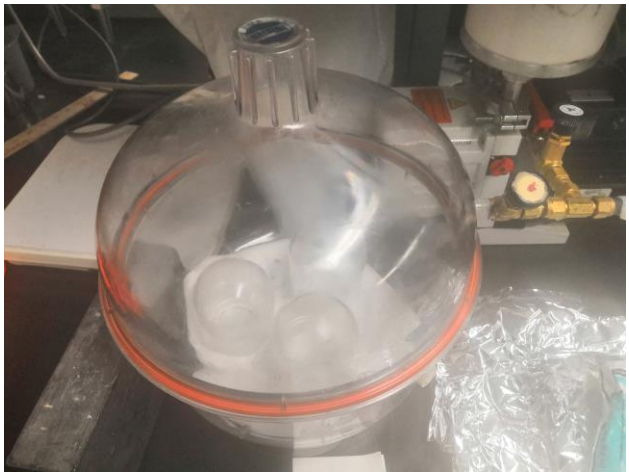

Epoxy encapsulation: Vacuum oven setup to for epoxy curing preparation

Sputtering: Au/Pd sputtering tool used to coat sample before SEM analysis.

APPENDIX C

SEM & EDXS CHARACTERIZATION TOOL

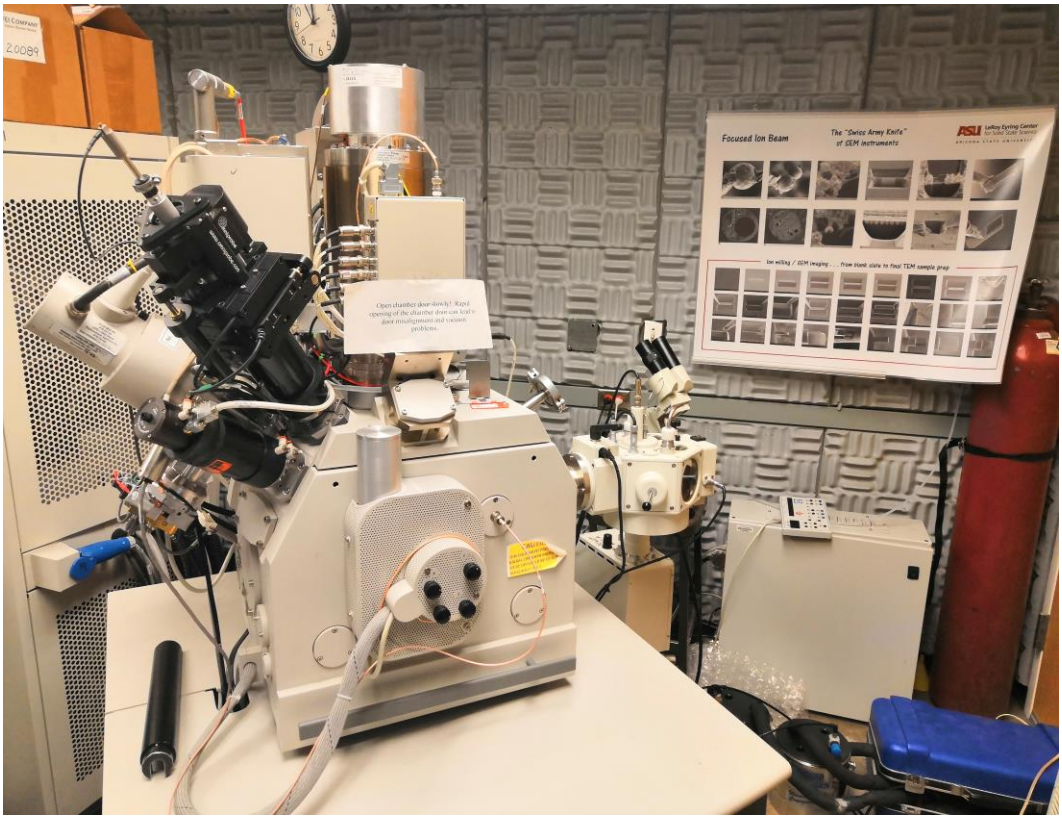

NOVA 200 Nanolab(FEI) Focused Ion Beam(FIB)/SEM dual column instrument with in-built EDXS detector.